



# Synthesis of Gd<sub>2</sub>O<sub>3</sub> nanoparticles: using bulk Gd<sub>2</sub>O<sub>3</sub> powders as precursor

Taher Yousefi\*, Meisam Torab-Mostaedi,  
Mostafa Ghasemi, Amir Ghadirifar

Received: 14 February 2014/Revised: 18 April 2014/Accepted: 13 January 2015/Published online: 5 February 2015  
© The Nonferrous Metals Society of China and Springer-Verlag Berlin Heidelberg 2015

**Abstract** Gd<sub>2</sub>O<sub>3</sub> nanoparticles were synthesized from the commercial bulk Gd<sub>2</sub>O<sub>3</sub> powders via a simple electrochemical method. The synthesized powders were characterized by means of X-ray powder diffraction (XRD), scanning electron microscopy (SEM), transmission electron microscopy (TEM) and Fourier transform infrared (FTIR) spectroscopy. The effects of solution pH on the morphological features of the sample were studied. The strategy developed in this study offers significant advantages for the synthesis of Gd<sub>2</sub>O<sub>3</sub> nanoparticles from the bulk Gd<sub>2</sub>O<sub>3</sub> powders compared with the conventional routes. From SEM observations, the size of the Gd<sub>2</sub>O<sub>3</sub> nanoparticles is estimated to be significantly smaller than 70 nm.

**Keywords** Gd<sub>2</sub>O<sub>3</sub>; Nanoparticles; Electro-deposition; Nanostructures

## 1 Introduction

Materials reduced to nanoscale can suddenly show a variety of properties compared with those in microscale due to two effects [1]. First, from the view point of surface effects, there are more surface atoms than the inner atoms and more free energy surface available (the increased surface area and surface atoms result in an increase in surface energy associated with the particles). Moreover, we should bear in mind the fact that increasing the surface area of substance generally increases the rate of chemical reaction. Second,

as regards the volume effects, the lower wavelengths (higher frequency and higher energy) lead to blue shift of atoms for optical absorption spectra and super-paramagnetism occurs when the particle is smaller than the magnetic domain in material. Another important aspect is that in a free electron model, the average energy spacing increases as the number of atoms is reduced, which enhances the catalytic properties of the nanoparticles [2].

The main objective of the nanoscale science and technology is to synthesize nanomaterials with controlled size and shape [3]. The shape of nanostructures is an important determinant of their physical and chemical properties; different shapes often display different surface structures and always expose different active planes. It is clear that the shape of nanostructure can control its properties and has usefulness in a given application [3]. The morphology and structure of a material depend upon synthetic conditions and parameters; therefore, many techniques were reported to synthesize materials bearing various geometries. Zhang et al. [3] provided a comprehensive study on the shape-controlled synthesis methods of ceria nanostructures. They presented the controlled synthesis of nanostructures based on different synthesis strategies, such as oriented growth directed by the crystallographic structure, oriented growth directed by the use of an appropriate capping reagent, growth confined or dictated by various templates and other potential methods. The capping reagents are selectively absorbed on specific facets of nanocrystals and direct their growth. Generally, three types of templates were used in the previous studies: self-template, soft template (surfactants) and hard template (porous solids such as carbon or silica). In the self-template, an initially formed nanocrystal is used as a template for the consequent aging and directed growth. In the soft template synthesis, the surfactants are often used as soft templates in

T. Yousefi\*, M. Torab-Mostaedi, M. Ghasemi, A. Ghadirifar  
Nuclear Fuel Cycle Research School, Nuclear Science and  
Technology Research Institute, 14395-836 Tehran, Iran  
e-mail: taher\_yosefy@yahoo.com

the preparation of nanostructures. In the case of hard templates, the porous material forms in a confined space due to the porosity of the template.

Gd<sub>2</sub>O<sub>3</sub> nanostructures obviously attract the interest of associated scholars due to their importance in basic scientific research and potential technology applications owing to their size effect and their promising application in nanoscale devices. It is one of the largest elements used in the nuclear power as shielding and fluxing devices. They are used, in general, electric boiling water reactor as burnable poison [4]. They mix directly with uranium to achieve a uniform neutron flux during the lifetime of a fuel element. Because of their broad range of potential applications, the development of simple synthetic methods including high-yield and shape-controlled Gd<sub>2</sub>O<sub>3</sub> nanostructures under mild conditions is of key importance [5]. Herein, a convenient route for the large-scale synthesis of uniform Gd<sub>2</sub>O<sub>3</sub> nanoparticles was reported using inexpensive bulk of Gd<sub>2</sub>O<sub>3</sub> in the absence of the capping and surfactant agent via electrochemical and heat-treatment. Different methods were developed to synthesize a variety of nanostructures, such as sol-gel process, reverse micelles, homogeneous precipitation, microwave, hydrothermal methods, spray pyrolysis and combustion [6–9]. However, there are several disadvantages of using these methods for the synthesis of such materials. For example, they are poorly crystallized and extensively agglomerated. Furthermore, they produce only subgram of products. Electro-deposition is a powerful and interesting process that can be applied in numerous fields. Films and powders can be synthesized at low temperature by electro-deposition because of the high energy density accumulated in solution near the electrode surface. The advantages of electro-deposition compared with other techniques include low process temperature, low cost for raw materials and equipment, capability of controlling composition and morphology by electrochemical parameters. In this paper, a cathodic electro-deposition and subsequent heat-treatment method for the preparation of Gd<sub>2</sub>O<sub>3</sub> nanoparticles was reported.

## 2 Experimental

All chemicals used were as received without further purification. H<sub>2</sub>O was distilled. Gd<sub>2</sub>O<sub>3</sub> was purchased from Merck. Commercial bulk Gd<sub>2</sub>O<sub>3</sub> powders of 0.5 g was dissolved in concentrated hydrochloric acid (36 %). The pH was adjusted with the NaOH aqueous solution. The specimen (60 mm × 30 mm × 1 mm), cut from commercial steel (316 L), was used as the substrate of the cathode. Prior to the deposition, the substrates were cleaned with detergent and diluted hydrochloric acid and

were then rinsed with distilled water. In the electrochemical cell for deposition, the cathode (steel) was centered between the two parallel graphite anodes. The electro-deposition was carried out by applying constant potential of 4 V for 10 min. Thermal annealing was conducted in air between the room temperature and 700 °C at heating rate of 10 °C·min<sup>-1</sup>.

The commercial bulk Gd<sub>2</sub>O<sub>3</sub> powders and Gd<sub>2</sub>O<sub>3</sub> nanoparticles were characterized by X-ray diffraction (XRD, Phillips, PW1800), scanning electron microscopy (SEM, LEO 1455VP), transmission electron microscopy (TEM, Phillips EM 2085) and Fourier transform infrared (FTIR) spectroscopy recorded with KBr pellet on VECTOR-22 (Bruker) spectrometer ranging from 400 to 4,000 cm<sup>-1</sup>. The measurement of specific surface area for the prepared sample was taken by measuring N<sub>2</sub> adsorption-desorption isotherms at 77 K with Quanta-chrome NOVA-2200e system.

## 3 Results and discussion

### 3.1 Deposition mechanism

The mechanism of metal hydroxides/oxides deposition (Fig. 1) is the basis of OH<sup>-</sup> generation at the electrode surface [10–15]. Contrary to the nitrate bath, the anions in the chloride bath do not participate in cathodic reaction; the hydroxyl ions are produced by the reduction of dissolved oxygen or water as shown in the following reactions.



The presence of OH<sup>-</sup> on the electrode surface causes the local increase in pH and the deposition of metal ions as hydroxide/oxide [10–15]:

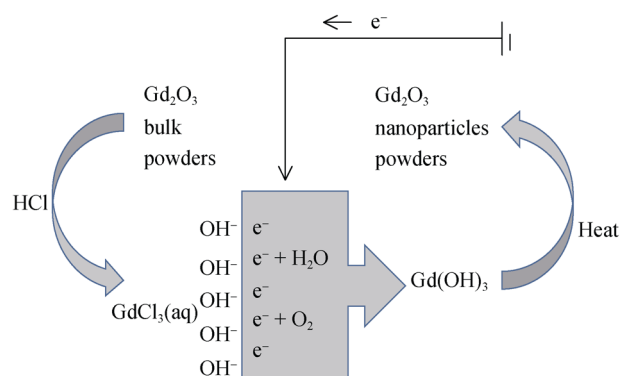
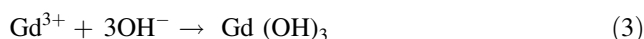
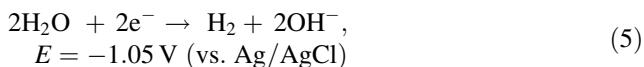
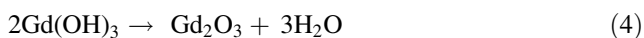


**Fig. 1** Formation mechanism of Gd<sub>2</sub>O<sub>3</sub> nanoparticles from Gd<sub>2</sub>O<sub>3</sub> bulk powder

The gadolinium hydroxide is converted to gadolinium oxide according to the following reactions:



### 3.2 Morphology analysis

Figure 2 shows representative SEM images of the precursor (Fig. 2a, b) and as-made samples (Fig. 2c, d), and TEM image of the sample (Fig. 2e). On the basis of these SEM results,  $\text{Gd}_2\text{O}_3$  micrometer precursor converts to nanoparticles at relatively low temperatures by electrochemical method. The average size of the precursor is about  $3 \mu\text{m}$ , while the synthesized sample is regularly shaped particles with the average size of less than  $70 \text{ nm}$ . Each particle consists of agglomeration of small particles with individual particle size of about  $5 \text{ nm}$ . In order to study the impact of pH on  $\text{Gd}_2\text{O}_3$  nanoparticles, the pH of the solution was adjusted by adding the required quantity of sodium hydroxide before commencing the reaction. The results show that the crystallinity degrees of samples prepared with different pH are almost the same. Figure 3 shows the surface morphologies of  $\text{Gd}_2\text{O}_3$  powders synthesized at pH of 6.3, 7.2 and 9.6. As can be seen, the morphologies of the obtained samples at different concentrations of NaOH are completely different from those

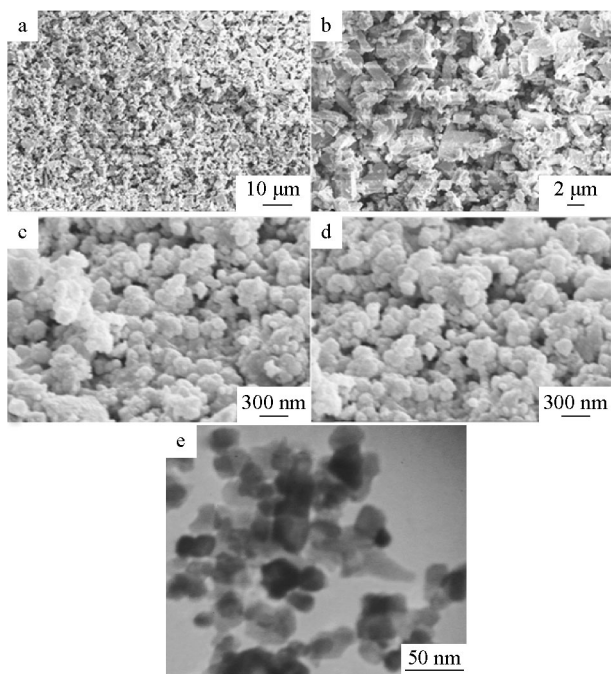


**Fig. 2** SEM images of precursor **a, b** and as-made sample **c, d**; TEM image of sample **e**

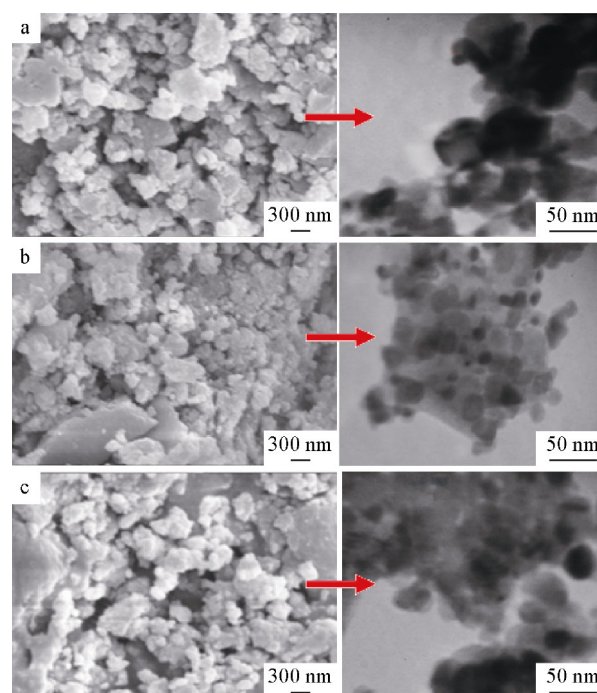


**Fig. 3** SEM and TEM images of  $\text{Gd}_2\text{O}_3$  nanoparticles prepared at different pH: **a** pH 6.3, **b** pH 7.2 and **c** pH 9.6

of the one without NaOH, and the morphology observed is more uniform for the latter. However, the morphologies of the samples in different concentrations of NaOH are almost the same (Fig. 3a–c). The SEM and TEM images show a slight change in morphology; the irregular particles grow together, although the shapes and cracks of particles in the samples with various NaOH concentrations are the same; with the increase of pH, the number of particles decreases, the size of the particles at higher pH values is bigger, and more particles agglomerate. Accordingly, it can be concluded that in cathodic deposition, the pH has a negligible effect on the sample morphology, because in cathodic deposition, the electro-generated hydroxide ions at a local area near the electrode surface are predominant and the solution hydroxide ions have an insignificant effect on it.

It is also noted that, as NaOH concentration increases, the weight, density and adhesion of deposition on the electrode reduce considerably; in fact, a negligible amount of depositions with weak adhesion are obtained at high pH compared with at low pH solution. This result can be described by Zeta potential (Fig. 4). The Zeta potential is a function of the surface charge, which develops when any material is placed in liquid. It is an index of the magnitude of the electrostatic repulsive interaction between particles.

During the formation of deposition, the particles become closer to each other; and with attraction force increasing, if

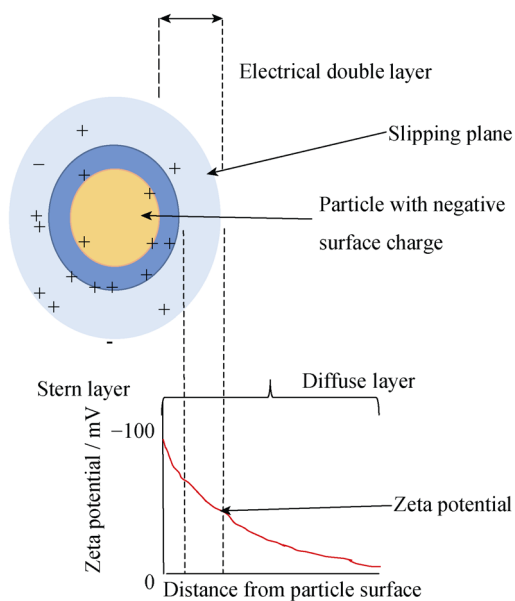
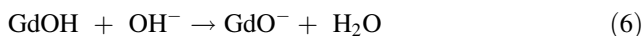


**Fig. 4** Schematic illustration of Zeta potential around particle

the particle charge is low, the particles would coagulate, leading to the formation of deposition. On the contrary, if the particles have a high surface charge, they will repulse each other, resulting in the suspension of particles in solution. In other words, if the particles have a considerably negative or positive Zeta potential, they will tend to repel each other and there is no tendency to form deposition. The charge magnitude or Zeta potential of particles can be controlled by a variety of charging agents such as acids, bases and specifically adsorbed ions.

Under alkaline conditions, the additional OH<sup>-</sup> reacts with hydroxide molecules and produces GdO<sup>-</sup>, as shown in the following reaction:



It seems that in alkaline condition, the negative Zeta potential is high and the GdO<sup>-</sup> molecules repel each other and prevent the deposition due to the formation of GdO<sup>-</sup>.

### 3.3 XRD results

Figure 5 is XRD patterns of the prepared Gd<sub>2</sub>O<sub>3</sub> material annealed at 700 °C. As shown in Fig. 5, the main diffraction peaks are positioned at 2θ = 28.63°, 33.12°, 47.59° and 56.43°, corresponding to (222), (400), (440) and (622) planes of the cubic Gd<sub>2</sub>O<sub>3</sub> phase (JCPDS 00-011-0604), respectively. According to Scherrer's equation, when the maximum peak broadens, the crystalline size will decrease. The full width at half maximum (FWHM) and the intensity of the maximum peak for the obtained nanoparticle are shown in Table 1. Crystalline size was calculated by Scherrer's equation [16]:

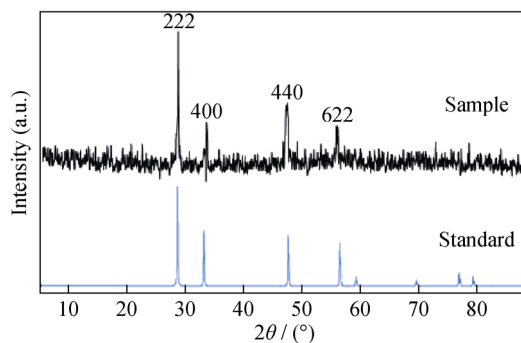


**Fig. 5** XRD patterns of sample

**Table 1** Average grain sizes of sample

Peak position (2θ)/(°)	FWHM/(°)	Intensity/cps	Particle size/nm
28.63	0.2509	412.11	32.5
33.12	0.4723	98.93	17.5
47.59	0.2804	197.46	31.0
56.43	0.2952	109.85	30.4

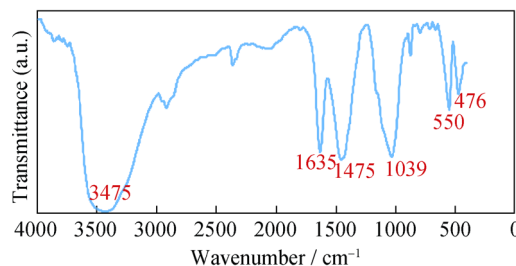


**Fig. 6** FTIR spectrum of sample

**Table 2** Vibrational mode assignments of Gd<sub>2</sub>O<sub>3</sub> nanoparticles

Assignments	Peak position/cm <sup>-1</sup>
Gd-O vibration mode of cubic Gd <sub>2</sub> O <sub>3</sub>	476
	550
CO <sub>3</sub> <sup>2-</sup> vibration mode	1,039
	1,475
O-H deformation vibration	1,635
O-H stretching vibration	3,475

$$D_{hkl} = 0.89\lambda / \beta_{hkl} \cos \theta \quad (7)$$

$$\beta_{hkl} = \Delta 2\theta \times \pi / 180^\circ \quad (8)$$

where  $D_{hkl}$  denotes average crystal size,  $\lambda$  is the wavelength of the incident X-rays (0.15406 nm),  $\theta$  is the diffraction angle,  $\beta_{hkl}$  is the measured half-width [16]; as summarized in Table 1. It is found that the crystallite size varies from 17.0 to 32.5 nm, denoting that nanoparticle powders form.



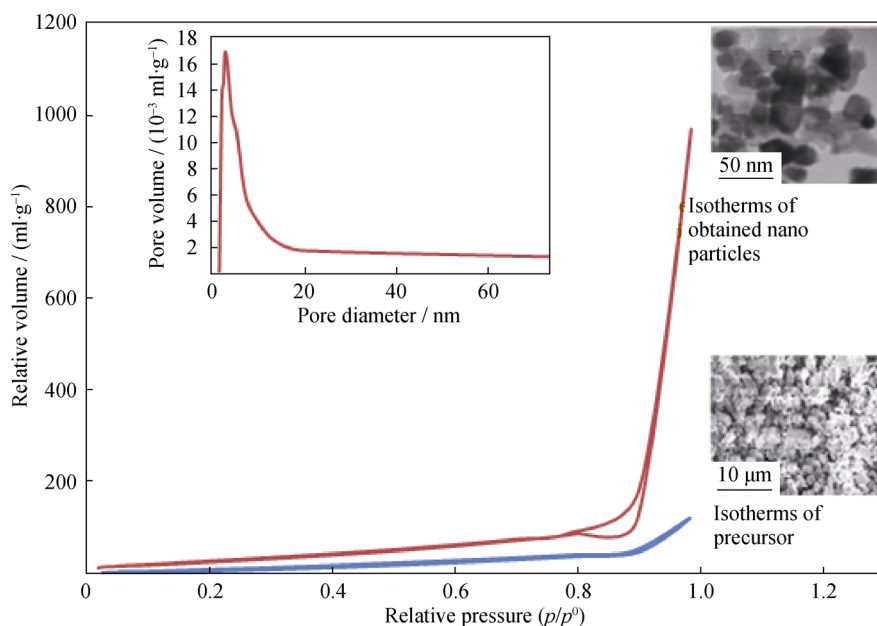


**Fig. 7**  $N_2$  adsorption–desorption isotherms curves of precursor and  $Gd_2O_3$  nanoparticles. Insert curve and images being Barrett–Joyner–Halenda (BJH) pore size distribution and SEM images of  $Gd_2O_3$  nanoparticles, respectively

### 3.4 FTIR results

Figure 6 shows the FTIR transmission spectrum of  $Gd_2O_3$  heat-treated at 700 °C. Assignments of vibrational modes observed for the samples are given in Table 2. The bands around 3,475 and 1,635  $cm^{-1}$  are due to the vibrations of O–H stretching and O–H deformation, respectively. The bands around 550 and 476  $cm^{-1}$  are assigned to the Gd–O vibration of cubic  $Gd_2O_3$ , which is in agreement with the results in Ref. [17]. In this situation, the contact of trapped water in the deposition with  $CO_2$  could lead to the formation of carbonate species characterized by a peak situated at 1,475 and 1,039  $cm^{-1}$  [18–20].

### 3.5 BET results

The nanostructure nature of the obtained sample is further validated by  $N_2$  adsorption/desorption isotherms. The Brunauer–Emmett–Teller (BET) surface area and porosity were investigated by nitrogen adsorption/desorption isotherms at 77 K (Fig. 7). Before adsorption measurements, the sample was activated by heating to 423 K with heating rate of 0.5  $K \cdot min^{-1}$  and keeping it at this temperature under the turbomolecular pump vacuum. The adsorption–desorption isotherm of the prepared  $Gd_2O_3$  exhibits Type IV isotherms with H1 hysteresis loop at relative pressure between 0.2 and 0.9. A specific surface area of  $Gd_2O_3$  nanoparticles (estimated from the BET method) is 116  $m^2 \cdot g^{-1}$ , which is much higher than that of precursor (38  $m^2 \cdot g^{-1}$ ) and is in good agreement with morphology results. In combination with the analysis based on TEM

and SEM images, it is reasonable to believe that the high surface area of  $Gd_2O_3$  nanoparticles is due to its small crystal grains, which give rise to a porous architecture. The pore size distribution of  $Gd_2O_3$  is shown in Fig. 7 (inset). According to International Union of Pure and Applied Chemistry (IUPAC) nomenclature, the sizes of micropores, mesopores, and macropores are less than 2 nm, between 2 and 50 nm, and greater than 50 nm in diameters, respectively. For the obtained  $Gd_2O_3$ , a narrow peak with mean pore widths of around 7 nm appears, indicating that the sample contains mesopores.

## 4 Conclusion

In this work, a very simple convenient electrochemical route was worked out for preparing gadolinium oxide nanoparticles. The  $Gd_2O_3$  nanoparticles were successfully synthesized via cathodic deposition method using commercial bulk  $Gd_2O_3$  powder precursor under the milder conditions without any catalysts or templates. The SEM, FTIR and XRD results confirm that  $Gd_2O_3$  nanoparticles form. This research shows that pH condition of the cathodic deposition (contrary to chemical methods) does not play a very significant role in controlling the characteristics of the product. The particle sizes are in the range of 10–70 nm. A critical point in this method is the electro-generation rate of  $OH^-$ , which affects the growth and the nucleation of the particles. The products were measured by XRD and TEM, and the average particle size is less than 70 nm.

**Acknowledgments** This study was financially supported by the Nuclear Science and Technology Research Institute of Iran.

## References

- [1] Macwan DP, Dave PN, Chaturvedi S. A review on nano-TiO<sub>2</sub> sol-gel type syntheses and its applications. *J Mater Sci.* 2011;46(11):3669.
- [2] Khajeh M, Laurent S, Dastafkan K. Nanoadsorbents: classification, preparation, and applications (with emphasis on aqueous media). *J Am Chem Soc.* 2013;113(10):7728.
- [3] Zhang D, Du X, Shi L, Gao R. Shape-controlled synthesis and catalytic application of ceria nanomaterials. *Dalton Trans.* 2012;41(48):14455.
- [4] Goldstein L, Strasser AA. A comparison of gadolinia and boron for burnable poison applications in pressurized water reactors. *Nucl Technol.* 1983;60(3):352.
- [5] Dakhel AA. Optical and dielectric properties of gadolinium-indium oxide films prepared on Si (100) substrate. *Chem Phys Lett.* 2004;393(4–6):528.
- [6] Luo JM, Xu JL, Zhong ZC. Microstructure and properties of Y<sub>2</sub>O<sub>3</sub>-doped steel-cemented WC prepared by microwave sintering. *Rare Met.* 2013;32(5):496.
- [7] Fredrik S, Henrik P, Rodrigo MPJ, Per-Olov K, Kajsa U. Synthesis and characterisation of Gd<sub>2</sub>O<sub>3</sub> nanocrystals functionalised by organic acids. *J Colloid Interface Sci.* 2005;288(1):140.
- [8] Bazzi R, Flores MA, Louis C, Lebbou K, Zhang W, Dujardin C, Roux S, Mercier B, Ledoux G, Bernstein E, Perriat P, Tillement O. Synthesis and properties of europium-based phosphors on the nanometer scale: Eu<sub>2</sub>O<sub>3</sub>, Gd<sub>2</sub>O<sub>3</sub>:Eu, and Y<sub>2</sub>O<sub>3</sub>:Eu. *J Colloid Interface Sci.* 2004;273(1):191.
- [9] Rahman ATMA, Vasilev K, Majewski P. Ultra small Gd<sub>2</sub>O<sub>3</sub> nanoparticles: absorption and emission properties. *J Colloid Interface Sci.* 2011;354(2):592.
- [10] Yousefi T, Davarkhah R, Golikand AN, Mashhadizadeh MH. Synthesis, characterization, and supercapacitor studies of manganese (IV) oxide nanowires. *Mater Sci Semicond Process.* 2013;16(3):868.
- [11] Yousefi T, Golikand AN, Mashhadizadeh MH, Aghazadeh M. Template-free synthesis of MnO<sub>2</sub> nanowires with secondary flower like structure: characterization and supercapacitor behavior studies. *Curr Appl Phys.* 2012;12(1):193.
- [12] Yousefi T, Golikand AN, Mashhadizadeh MH, Aghazadeh M. High temperature and low current density synthesis of Mn<sub>3</sub>O<sub>4</sub> porous nano spheres: characterization and electrochemical properties. *Curr Appl Phys.* 2012;12(2):544.
- [13] Yousefi T, Golikand AN, Mashhadizadeh MH, Aghazadeh M. Facile synthesis of α-MnO<sub>2</sub> one-dimensional (1D) nanostructure and energy storage ability studies. *J Solid State Chem.* 2012;190:202.
- [14] Yousefi T, Golikand AN, Mashhadizadeh MH, Aghazadeh M. Hausmannite nanorods prepared by electrodeposition from nitrate medium via electrogeneration of base. *J Taiwan Inst Chem Eng.* 2012;43(4):614.
- [15] Zhitomirsky I. Cathodic electrodeposition of ceramic and organoceramic materials. Fundamental aspects. *Adv Colloid Interface Sci.* 2002;97(1–3):279.
- [16] Tok AIY, Boey FYC, Dong Z, Sun XL. Hydrothermal synthesis of CeO<sub>2</sub> nano-particles. *J Mater Process Technol.* 2007;190(1–3):217.
- [17] Gao H, Yang X, Xiao T, Zhang W, Lou L, Mugnier J. Structure and optical properties of sol-gel derived Gd<sub>2</sub>O<sub>3</sub> waveguide films. *Appl Surf Sci.* 2004;230(1–4):215.
- [18] Hamlaoui Y, Pedraza F, Tifouti L. Investigation of electrodeposited cerium oxide based films on carbon steel and of the induced formation of carbonated green rusts. *Corros Sci.* 2008;50(8):2182.
- [19] Djuricic B, Pickering S. Nanostructured cerium oxide: preparation and properties of weakly-agglomerated powders. *J Eur Ceram Soc.* 1999;19(11):1925.
- [20] Siokou A, Ntais S, Dracopoulos V, Papaefthimiou S, Leftheriotis G, Yianoulis P. Substrate related structural, electronic and electrochemical properties of evaporated CeO<sub>x</sub> ion storage layers. *Thin Solid Films.* 2006;514(1–2):87.